Emergent spatiotemporal instabilities in reactive spatially extended systems by thermodiffusion

Pushpita Ghosh *
Tata Institute of Fundamental Research, Hyderabad 500107, India

(Received 26 August 2019; published 25 October 2019)

Thermodiffusion or thermophoresis or Soret effect, i.e., mass-transport induced by thermal gradient, has immense application in segregation of species in two or multicomponent gaseous, liquid, or colloidal mixtures. Here, we show that an external thermal gradient can be effectively utilized in creation and modification of patterns in spatially extended systems. We consider Brusselator and chlorine-dioxide iodine malonic acid (CDIMA) reaction-diffusion systems, which follow activator-inhibitor kinetics subjected to an external thermal gradient. We find that the conspicuous interaction of emergent thermodiffusive flux with reaction kinetics and diffusion can lead to various spatiotemporal instabilities in these two models. Specifically, our result reveals formation of Turing-like spatial patterns even for equal diffusivities of the activator and inhibitor components in the Brusselator model under the influence of differential thermodiffusion, whereas formation of such stationary patterns in the CDIMA system from a homogenous stable steady state, which is also stable under differential diffusion, requires the same sign and magnitude of Soret coefficients. However, with equal diffusivities of the components of the CDIMA system and without starch in the medium, our result identifies formation of drifting spiral waves which finally disappears at longer times under the influence of thermodiffusion. We also show formation of propagating patterns of spotlike or stripelike heterogeneity in both the model systems under appropriate conditions. Our study provides a route to pattern formation beyond Turing space and reveals remarkable influence of thermodiffusion to modify the pattern types just by employing an external thermal gradient which also opens up the possibility to set up new related experiments.

DOI: 10.1103/PhysRevE.100.042217

I. INTRODUCTION

The spontaneous formation of patterned structures is one of the most fascinating far-from-equilibrium phenomena which has received significant attention for decades due to its prevalent occurrence in many naturally evolving spatially extended systems [1–4]. The most common mechanism of spatiotemporal pattern formation was proposed in early 1950s by mathematician Alan Turing in the context of morphogenesis [5], which suggests that, in a system of two interacting and diffusing species, the disparity between diffusion coefficients of activator and inhibitor might lead to the formation of stable heterogeneous spatial patterns. This is well known as Turing instability or diffusion-driven instability. Nevertheless, it is hard to achieve such a large difference of diffusivities between two interacting chemical species in chemical reactions in real experiments; a large number of studies have been reported so far in this context to investigate pattern formation processes both theoretically and experimentally [6–11]. Efforts had been made in literature to overcome the stringent criteria of equal diffusivities to generate spatiotemporal instabilities by externally perturbing the chemical reaction-diffusion systems using differential flow [12], electric fields and magnetic fields [13–17], photoillumination [18,19], or by including time-delay and time-delayed feedbacks [20,21] or fluctuations in different forms [22–27]. In the same line, the problem of equal diffusion coefficients has been addressed in reaction-diffusion systems with cross-diffusion [28] and diffusion on complex networks [29].

In this regard, we investigate here the spatiotemporal dynamics of a reaction-diffusion system subjected to an externally applied temperature gradient. A thermal gradient in a fluid mixture not only causes heat flux but also generates a diffusive flux of the constituent components and thereby influences the overall transport. This phenomenon of mass transport driven by temperature gradients in binary or multicomponent fluid mixtures is known as thermodiffusion [30–34] or Ludwig-Soret effect, which was first observed in 1856 by Ludwig and later established by Soret in 1979. This cross effect between temperature and concentration can be naturally found in thermohaline convection in oceans, in segregation of components in liquid lava. Use of thermal diffusion has been found in separation of metals in alloys and for purification of isotopes [35–37]. Thermal diffusion has been explicitly studied in complex molecular systems such as colloidal suspensions and charged micelles [36,38–42]. Although, previously, Soret effect has been studied in a reactive one-component spatially extended system resulting in absolute and convective instabilities [43] and unpinning of scroll waves in B-Z reaction [44], a systematic investigation of thermodiffusion induced spatial instability in spatially extended systems is still elusive.

In this paper, we study how and to what extent an applied external thermal gradient influences the spatiotemporal dynamics of a planar two-component spatially extended system following activator-inhibitor kinetics. As prototypical examples we consider two dynamical systems: Brusselator

*pghosh@tifrh.res.in

model and chlorine-dioxide iodine malonic acid (CDIMA) system [7,45,46]. The focal theme of the paper concerns thermodiffusion-induced pattern formation in the presence or absence of diffusion-driven instability. In what follows, we show that thermodiffusion can lead to the emergence of spatiotemporal instabilities in the form of Turing-type stationary patterns and traveling waves in general depending on the appropriate parameter region and Soret coefficients. Our theoretical analysis is corroborated with numerical simulations done for the two aforementioned model systems. However, the spatiotemporal dynamics of the two systems have certain distinct features under the influence of external thermal gradient. While, our study identifies formation of a stationary pattern even for equal diffusivities in the presence of differential thermodiffusion of the components in the Brusselator model, in the case of the CDIMA system, without disparity in diffusion, thermal gradient alone is inadequate to generate stationary Turing patterns. However, Soret coefficients of the same sign and magnitude result in stationary patterns in the CDIMA system from a homogeneous stable state in the presence of diffusion-driven instability. Interestingly, in the CDIMA system, opposite signs or difference in magnitude of Soret coefficients always generate propagating patterns of spot- or striplike heterogeneity or spiral waves. Based on the knowledge of existing literature, these thermodiffusion-induced stationary patterns are reported in two-component reaction-diffusion systems in the present study in addition to various propagating patterns. Along with other chemical reactions, our study can be useful to investigate collective spatiotemporal dynamics of fish school in the ocean, where temperature gradients might be present as well as thermosensitive microbial systems. Similarly, our study can be extended to investigate spatiotemporal dynamics of dust particles in atmosphere under the influence of temperature gradients.

The rest of the paper is organized as follows: in Sec. II, we provide a description to include the effect of thermodiffusive flux in a general reaction-diffusion model. In Sec. III we demonstrate, analyze, and discuss the results of the present work on the application of thermal gradient on Brusselator and chlorine-dioxide iodine malonic acid (CDIMA) reaction-diffusion system. The paper is concluded in Sec. IV.

II. ROLE OF THERMODIFFUSION: A GENERAL THEORETICAL DESCRIPTION

To investigate the influence of externally employed temperature gradient in a spatially expended system, we first consider a general reaction-transport model in two dimensions represented by the following equations:

$$\dot{u} = f(u, v) - \nabla \cdot J_u, \tag{1}$$

$$\dot{v} = g(u, v) - \nabla \cdot J_v, \tag{2}$$

where $u(x, y, t)$ and $v(x, y, t)$ are two dimensionless concentration variables. J_i denotes the flux of the ith species for the system. $f(u, v)$ and $g(u, v)$ are the reaction parts following activator-inhibitor kinetics. In the presence of an applied constant thermal gradient, the flux for a species is given by the Ludwig-Soret effect [30,33,35,36] as

$$J_i = -D_i \nabla c_i - D_{T_i} c_i (1 - r_i) \nabla T. \tag{3}$$

Here D_i is the translational diffusion coefficient, D_{T_i} denotes the thermal diffusion coefficient, c_i is the concentration of the ith species, and r_i is the relative concentration of the same (i.e., $r_i = c_i / \sum c_i$). ∇T is the imposed thermal gradient (can have a dimension K cm^{-1}), across the reaction chamber and is kept constant throughout. D_{T_i} can be expressed in the form $D_{T_i} = \mathbf{S}_{T_i} D_i$, $\mathbf{S}_{T_i}$ being the Soret coefficient having the dimension K^{-1}, of the ith species, which is expressed by the relation $\mathbf{S}_{T_i} = S_{T_i}(1 + k_s c_i)^{-1}$ [47]. Here k_s is a phenomenological constant (can be expressed in M^{-1} unit). The values of S_{T_i} are nearly equal for ionic species. Equation (3) can be written in the following form:

$$J_i = -D_i \nabla c_i - D_i S_{T_i} c_i \frac{(1 - \chi c_i)}{(1 + k_s c_i)} \nabla T, \tag{4}$$

where $r_i = \chi c_i$ and $\chi = 1 / \sum c_i$.

On substituting the expression of the total flux from Eq. (4) in Eq. (1) and Eq. (2) we get

$$\dot{u} = f(u, v) + D_u \nabla \cdot \left(\nabla u + S_{T_u} \frac{u(1 - \chi u)}{(1 + k_s u)} \nabla T \right), \tag{5}$$

$$\dot{v} = g(u, v) + D_v \nabla \cdot \left(\nabla v + S_{T_v} \frac{v(1 - \chi v)}{(1 + k_s v)} \nabla T \right). \tag{6}$$

The sign of the Soret coefficient decides the movement of a species towards the hot or cold ends. Those with positive coefficient move to the colder region and ones with negative Soret coefficient move towards the warmer region.

At this point, we examine the effect of thermodiffusion in modifying the instability region such that a homogeneous stable steady state which is stable otherwise becomes unstable in the presence of thermodiffusion. We now consider a small spatiotemporal perturbation around the homogeneous steady state (u_0, v_0) so that $u(x, y, t) = u_0 + \delta u(x, y, t)$ and $v(x, y, t) = v_0 + \delta v(x, y, t)$. By expanding u and v about the steady state value (u_0, v_0) and keeping only the linear terms we obtain

$$\frac{\partial(\delta u)}{\partial t} = f_u(\delta u) + f_v(\delta v) + D_u \nabla^2(\delta u) + D_u S_{T_u} \nabla T \left[\frac{1 - \chi_0 u_0}{(1 + k_s u_0)^2} - \frac{\chi_0 u_0}{(1 + k_s u_0)} \right] \nabla(\delta u), \tag{7}$$

$$\frac{\partial(\delta v)}{\partial t} = g_u(\delta u) + g_v(\delta v) + D_v \nabla^2(\delta v) + D_v S_{T_v} \nabla T \left[\frac{1 - \chi_0 v_0}{(1 + k_s v_0)^2} - \frac{\chi_0 v_0}{(1 + k_s v_0)} \right] \nabla(\delta v), \tag{8}$$

where the terms within the third brackets correspond to the first derivative of the Soret term at the steady state (u_0, v_0) and χ_0 equals the sum of the initial concentrations of the reactants.

Expressing the spatiotemporal perturbations in the form

$$\delta u(x, y, t) = (\delta u_0) e^{[\lambda t + i(k_x \cdot x + k_y \cdot y)]}, \tag{9}$$

$$\delta v(x, y, t) = (\delta v_0) e^{[\lambda t + i(k_x \cdot x + k_y \cdot y)]} \tag{10}$$

and substituting the above into Eq. (7) and Eq. (8), we obtain the following matrix equation for the eigenvalues:

$$\begin{pmatrix} f_u - D_u k^2 + ipD_u S_{T_u} M_u \nabla T - \lambda & f_v \\ g_u & g_v - D_v k^2 + ipD_v S_{T_v} M_v \nabla T - \lambda \end{pmatrix} \begin{pmatrix} \delta u_0 \\ \delta v_0 \end{pmatrix} = 0, \tag{11}$$

where $p = (k_x + k_y)$ and $k^2 = k_x^2 + k_y^2$. For the sake of simplicity we assume $M_u = [(1 - \chi_0 u_0)/(1 + k_s u_0)^2 - (\chi_0 u_0)/(1 + k_s u_0)]$ and $M_v = [(1 - \chi_0 v_0)/(1 + k_s v_0)^2 - (\chi_0 v_0)/(1 + k_s v_0)]$.

To determine the stability of the system we focus on the eigenvalue equation of the growth rate λ as obtained by expanding the stability matrix:

$$\lambda^2 - m\lambda + h = 0, \tag{12}$$

where $m = (f_u + g_v) - (D_u + D_v)k^2 + ip\nabla T(D_u S_{T_u} M_u + D_v S_{T_v} M_v)$ and $h = (f_u g_v - g_u f_v) - (f_u D_v + g_v D_u)k^2 + D_u D_v k^4 + ip\nabla T[(D_u S_{T_u} M_u g_v + D_v S_{T_v} M_v f_u) - D_u D_v k^2 (S_{T_u} M_u + S_{T_v} M_v)] - D_u D_v S_{T_u} S_{T_v} M_u M_v (\nabla T)^2 p^2$.

The eigenvalues of Eq. (12) are given by the expression

$$\lambda_\pm = [m \pm \sqrt{m^2 - 4h}]/2. \tag{13}$$

The eigenvalues consist of both real and imaginary parts. Deriving the expression $\sqrt{m^2 - 4h}$, we obtain the real part as represented by $R = \sqrt{(A + \sqrt{A^2 + B^2})/2}$ and the imaginary part $Q = B/\sqrt{2(A + \sqrt{A^2 + B^2})}$, where $A = [f_u + g_v - (D_u + D_v)k^2]^2 - 4[(f_u g_v - g_u f_v) - (f_u D_v + g_v D_u)k^2 + D_u D_v k^4] - (\nabla T)^2 (D_u S_{T_u} M_u - D_v S_{T_v} M_v)^2 p^2$ and $B = 2p\nabla T[f_u + g_v - (D_u + D_v)k^2][D_u S_{T_u} M_u + D_v S_{T_v} M_v] - 4p\nabla T[D_u g_v S_{T_u} M_u + D_v f_u S_{T_v} M_v - D_u D_v k^2 (S_{T_u} M_u + S_{T_v} M_v)]$.

The growth rate of perturbation, i.e., the eigenvalues, can be obtained by the following expression:

$$\mathrm{Re}(\lambda_\pm) = [\{f_u + g_v - (D_u + D_v)k^2\} \pm R]/2, \tag{14}$$

$$\mathrm{Im}(\lambda_\pm) = [p\nabla T(d_u S_{T_u} M_u + d_v S_{T_v} M_v) \pm Q]/2, \tag{15}$$

which determine the nature of the stability of the steady state. By plotting the three-dimensional (λ, k_x, k_y) dispersion diagram and identifying positive eigenvalues, we examine the effect of thermodiffusion in determining the instabilities.

In the next section we apply the aforementioned theoretical analysis considering two model reaction-diffusion systems. We consider a two-dimensional reaction chamber and maintain a no-flux boundary condition. The reason behind this choice of boundary condition is to corroborate with the possible experimental setup to maintain a constant temperature difference between two ends of the reaction chamber. A circular type of reactor with periodic boundary condition would not meet the present purpose. To obtain a constant thermal gradient across the reaction chamber, we need to first maintain a difference in temperature along the two opposite sides of the reaction chamber. For instance, in a square reaction chamber of length 10 cm, a 50 K difference in temperature will create a thermal gradient of 5 K cm^{-1}.

Our aim here is to investigate the following: how does the presence of an external thermal gradient (i) destabilize a homogeneous stable steady to generate stationary spatial patterns or propagating waves? and (ii) modify the type of instability in the form of pattern transition in a spatially extended system?

III. APPLICATIONS AND DISCUSSION

A. Brusselator model

To begin with, we first consider the Brusselator model which is a representative paradigm for autocatalytic chemical reactions [48,49]. The corresponding two variable reaction-diffusion model in the presence of an external thermal gradient can be described by two dimensionless equations as represented by Eq. (5) and Eq. (6) described in Sec. II, with the reaction terms having the form $f(u, v) = a - (b + 1)u + u^2 v$ and $g(u, v) = bu - u^2 v$. Here a and b are constant reaction parameters related to the reactant concentration.

The dynamical system represented by Eq. (5) and Eq. (6) with Brusselator kinetics admits a homogeneous steady state $(u_0 = a, v_0 = b/a)$, which is stable below a threshold, $b < b_H$, where $b_H = (1 + a^2)$ refers to the Hopf-bifurcation line obtained for parameters $D_v = 5.0$ and $a = 3.0$ and can be drawn as a function of diffusion coefficient of activator, i.e., D_u as shown in Fig. 1. This line separates the region of homogeneous stable steady states from oscillatory states in the $(b - D_u)$ parameter space. In the presence of simple diffusion of the components $(\nabla T = 0)$, the homogeneous steady state becomes unstable and diffusion-induced heterogeneous concentration patterns emerge following the Turing condition: $b_T = 1 + (a\sqrt{D_u/D_v})^2$ as derived from linear stability analysis. The region above the Turing curve and below the

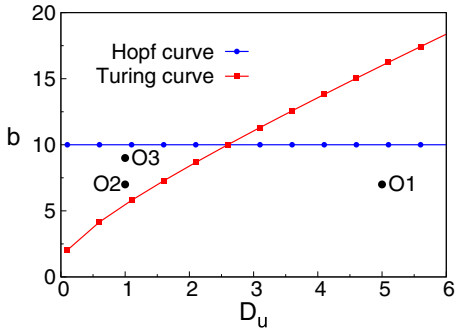

FIG. 1. Bifurcation diagram obtained from linear stability analysis of Eq. (5) and Eq. (6) with Brusselator kinetics in the absence of thermal gradient $(\nabla T = 0)$ and for $D_v = 5.0$ and $a = 3.0$. Hopf (blue) and Turing (red) curves divide the $(b - D_u)$ parameter space into a homogeneous stable region, a homogeneous oscillatory region, and a region of inhomogeneous stationary Turing patterns. The homogeneous stable steady states are denoted by points O1, O2, and O3 on the bifurcation diagram. O1 lying below both the Hopf and Turing curves is diffusionally stable and O2 and O3 inside the Turing region show stationary patterns.

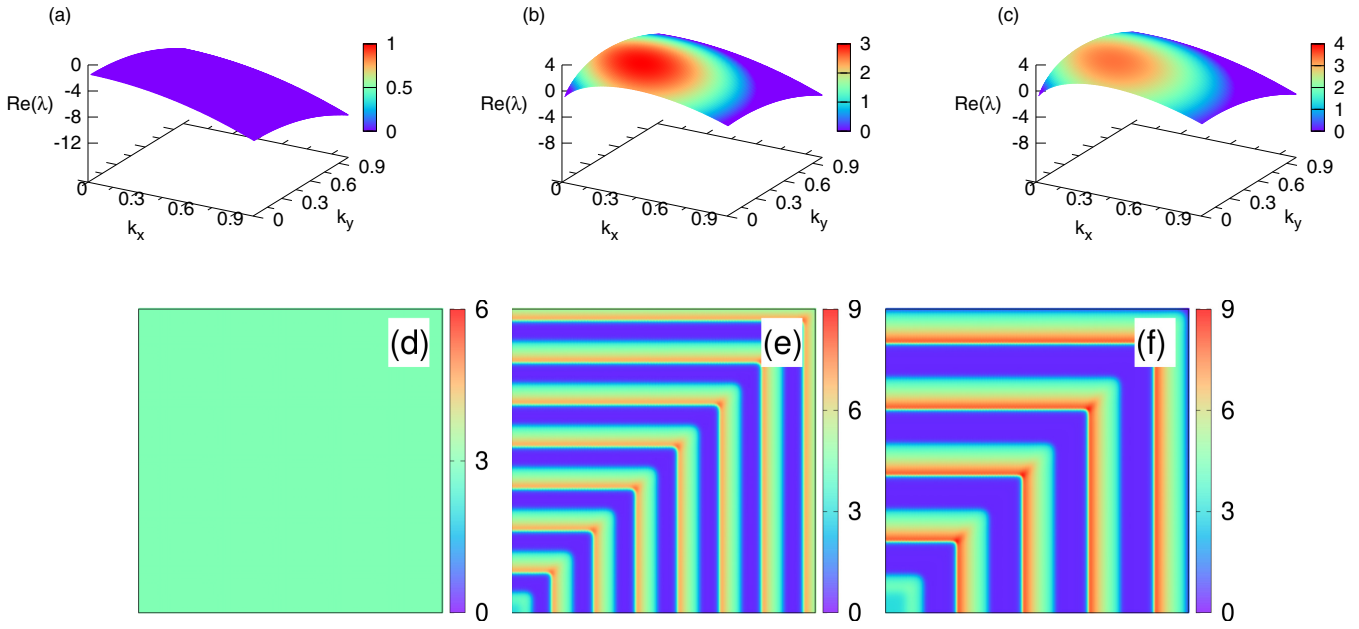

FIG. 2. Formation of Turing-like stationary patterns for equal diffusion coefficients of the two components ($D_u = D_v = 5.0$): a three-dimensional dispersion diagram for thermodiffusion induced instability is obtained from linear stability analysis for the state O1 for the Soret coefficients $S_{T_u} = 0.1$, $S_{T_v} = 0.5$. Shown here are the plots of the real part of the growth rate Re(λ) as a function of k_x and k_y for different values of the imposed temperature gradient: (a) $\nabla T = 0$, (b) $\nabla T = 4.0$, and (c) $\nabla T = 5.0$. All the other parameters are the same as mentioned in the main text. The corresponding numerically simulated spatial patterns of concentration of the activator u are depicted in bottom figures (d), (e), and (f), respectively.

Hopf curve as depicted in Fig. 1 is attributed to diffusion-driven instability. For further analysis we choose a point O1 ($D_u = 5, b = 7$) in the bifurcation diagram as shown in Fig. 1, which lies below both the Hopf and Turing curves representing a homogeneous stable steady state. Our aim here is to investigate the fate of the state O1 in the presence of an external thermal gradient, which does not show diffusion-driven Turing instability.

1. Formation of Turing-like stationary patterns for equal diffusivities ($D_u = D_v$)

To examine the influence of temperature gradient in inducing spatial instability of the homogeneous steady state corresponding to the point O1 in the bifurcation diagram 1, we first check the presence of real positive eigenvalues dominant over imaginary ones as given by Eq. (14) in Sec. II by drawing a three-dimensional dispersion diagram [Re(λ), k_x, k_y] for different values of thermal gradient ∇T. We consider equal diffusivity of the two components, i.e., $D_u = D_v = 5$, which does not fulfill the necessary condition of Turing instability. We now investigate spatiotemporal dynamics of the system considering Soret coefficients with positive sign and different magnitudes ($S_{T_u} = 0.1$, $S_{T_v} = 0.5$), which implies differential movement of the components towards the cooler part of the reaction chamber under thermodiffusion. The values of other parameters are $a = 3.0$, $D_v = 5.0$, $\chi = 1.0$, and $k_s = 0.1$, which we kept constant throughout our study unless otherwise mentioned. We observe no positive real eigenvalue for $\nabla T = 0$, as shown in Fig. 2(a). With increasing values of $\nabla T = 4.0$, we find the appearance of real positive eigenvalues as depicted in Fig. 2(b). Moreover, as ∇T increases, the magnitude of largest positive eigenvalue also increases [Fig. 2(c)], signifying formation of stable stationary patterns. The differential fluxes originated in response to the temperature gradient are the key for the development of this spatial instability.

To verify the predictions obtained from the 3D dispersion diagrams, we now perform detailed numerical integration of Eq. (5) and Eq. (6), following the Brusselator model in two dimensions for several values of imposed thermal gradients. For numerical simulations, an explicit Euler method is used following a discretization of space and time. A finite system size of length $L_x = L_y = 200$ with grid size $\Delta x = \Delta y = 0.5$ and a time interval $dt = 0.001$ are set for the present purpose. We maintain a no-flux boundary condition throughout our present study. The system is initialized at each mesh point (400×400 array) by perturbing the steady state with $\pm 1\%$ random noise in order to break the initial spatial symmetry. The numerical simulations are performed for a long time to observe the effect of the applied temperature gradient so that it can lead to the formation of stable heterogeneous patterns. Our numerical result shows a homogeneous uniform spatial pattern as depicted in Fig. 2(d) in the absence of any applied temperature gradient. As a thermal gradient is imposed on the system, we initially find transient patterns which finally become homogeneous. With increase in the value of $\nabla T \geqslant 4$, we observe formation of a stationary stripe pattern as illustrated in Fig. 2(e). Moreover, further increase of $\nabla T = 5.0$ results in a stationary spatial pattern of larger wavelengths that is clearly captured in Fig. 2(f). However, we find that in this case, when both the diffusion and Soret coefficients of the two components are equal, the system does not admit formation of a Turing-like stationary pattern in the presence of thermal gradient.

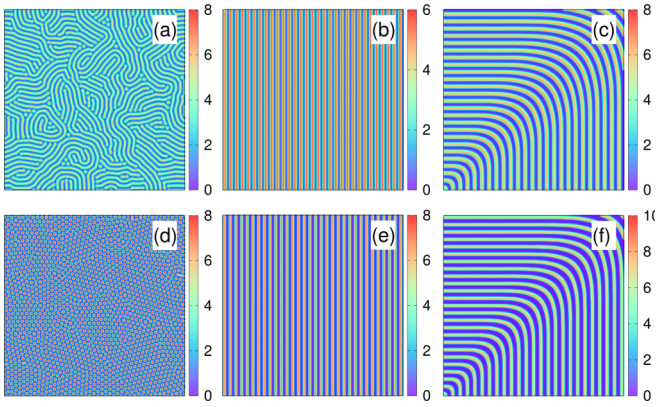

FIG. 3. Modulation of Turing patterns under thermodiffusion: plot of numerically simulated concentration patterns of activator u corresponding to the parameter set designated by point O2(1,7) are shown by the images (a)–(c) and point O3(1,9) are depicted in images (d)–(f) for different values of the imposed temperature gradient $\nabla T = 0.0$, $\nabla T = 2.0$, and $\nabla T = 4.0$, respectively. The Soret coefficients are taken as $S_{T_u} = S_{T_v} = 0.1$.

To this end, we now discuss the effect of thermodiffusion with negative Soret coefficients of the component species, i.e., when both the species are moving towards the hot end of the reactor. We carry out numerical simulations with the same parameter set referring point O1 as described earlier with $S_{T_u} = -0.1, S_{T_v} = -0.5$ for $\nabla T = 1.0$. Interestingly, in this case we observe wave instabilities in the form of traveling waves of stripelike heterogeneity as demonstrated in Movie 1 (see Supplemental Material [50]). However, for higher values of $\nabla T = 5$, we end up with a stationary pattern. On the other hand, with opposite signs of Soret coefficients for example either with $S_{T_u} = -0.1, S_{T_v} = 0.5$ or $S_{T_u} = 0.1, S_{T_v} = -0.5$ we find an oscillatory pattern of propagating periodic stripes. Therefore, by proper tuning of external applied thermal gradient, one can achieve patterns of varied wavelength and various types.

2. Modulation of Turing patterns in the presence of applied thermal gradient

To further explore how and to what extent an applied thermal gradient can influence the spatiotemporal dynamics of a patterned state we consider a point O2, lying inside the Turing region, as shown on the bifurcation diagram (Fig. 1). In absence of ∇T, numerical simulation of the system shows spatial heterogeneity in concentrations in the form of labyrinthine stripes as shown in Fig. 3(a). As ∇T is applied, imaginary eigenvalues appear and compete with the real ones and the system shows propagating spatial heterogeneity. For a larger $\nabla T = 2.0$, it turns out that positive real eigenvalues dominate over imaginary ones and by selection of a particular mode, stationary pattern of vertically oriented stripes is emerged as depicted in Fig. 3(b). For further increase of $\nabla T = 4.0$, again a transition occurs and stationary stable patterns of horizontally bent periodic stripes appear as shown in Fig. 3(c). A similar type of pattern transition from spots to stripes occurs in the presence of thermal gradient in the case of state described by point O3. Corresponding numerically simulated concentration patterns of activator component are demonstrated in Figs. 3(d)–3(f) for different values of applied thermal gradients. The underpinning of such transition reveals competition between real and imaginary eigenvalues of the growth rate of perturbation which results in some spatial patterns which consist of a mixture of stationary and oscillatory instabilities. Further exploration in the Turing domain reveals that in the presence of an applied thermal gradient either a propagating stripelike heterogeneous pattern evolves or a stationary pattern develops in the concentration fields even with negative Soret coefficients, e.g., $(S_{T_u} = S_{T_v} = -0.1)$. When components move in opposite directions with the same speed in response to applied thermal gradient in Turing space, propagating waves of stripes evolve in a particular direction for lower values of ∇T and stable stationary patterns emerge for higher values of ∇T. This signifies the potential role of thermodiffusion to manipulate the pattern types just by adjusting the value of the externally applied thermal gradient.

B. Chlorine-dioxide iodine malonic acid model

Next, we consider the chlorine-dioxide iodine malonic acid (CDIMA) model proposed by Lengyl and Epstein in 1992 [7,45,46] in the context of spatiotemporal instabilities in chemical reactions. This is a simple activator-inhibitor kind of model which has served as a representative paradigm for many experimental and theoretical studies on pattern formation over the past two decades [14,15,19–21,23,51]. The corresponding two-variable reaction-diffusion system in the presence of a thermal gradient can be written by the following dimensionless equations in two dimensions:

$$\dot{u} = f(u,v) + \nabla\cdot\left(\nabla u + S_{T_u}\frac{u(1-\chi u)}{(1+k_s u)}\nabla T\right), \quad (16)$$

$$\dot{v} = \sigma\left[g(u,v) + d\nabla\cdot\left(\nabla v + S_{T_v}\frac{v(1-\chi v)}{(1+k_s v)}\nabla T\right)\right], \quad (17)$$

where u and v refer to the activator I^- and the inhibitor ClO_2^-, respectively. The ratio of diffusion coefficients of inhibitor and activator is denoted by $d = D_{ClO_2^-}/D_{I^-}$. The constant σ refers to the concentration of starch which forms a complex with tri-iodide I_3^- such that $\sigma = 1 + K[S]$ and K is the equilibrium constant of the starch-iodide complex and $[S]$ is the concentration of starch tri-iodide binding sites. Here, $f(u,v) = [a - u - 4uv/(1+u^2)]$ and $g(u,v) = b[u - uv/(1+u^2)]$ are the dimensionless reaction kinetic terms which govern the dynamics of u and v in the absence of diffusion and any external flux. a and b are the kinetic parameters corresponding to the concentrations of the reactants, i.e., malonic acid (MA), I_2, and ClO_2 and are represented by $a = [MA]/[I_2]$ and $b = [ClO_2]/[I_2]$.

The dynamical system given by Eq. (16) and Eq. (17) admits a homogeneous steady state $(u_0 = a/5, v_0 = 1 + a^2/25)$ so that $f(u_0, v_0) = g(u_0, v_0) = 0$. The steady state is stable above a critical threshold such that $b > b_H$, where $b_H = [(3a/5 - 25/a)/\sigma]$ refers to the Hopf-bifurcation curve which separates the homogeneous stable steady state from the unstable oscillatory state. In the presence of simple diffusion, this homogeneous stable steady state becomes unstable and diffusion-driven instability comes into play under the

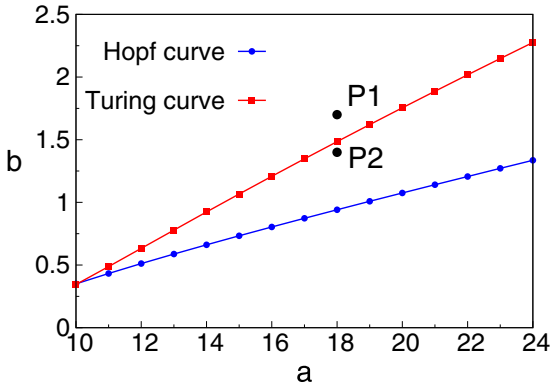

FIG. 4. Bifurcation diagram obtained from linear stability analysis of Eq. (16) and Eq. (17) in the absence of thermal gradient ($\nabla T = 0$) and for $d = 1.6$ and $\sigma = 10.0$. Hopf (blue) and Turing (red) curves divide the $(a - b)$ parameter space into a homogeneous stable region, a homogeneous oscillatory region, and a region of inhomogeneous stationary Turing patterns. The two homogeneously stable steady states are denoted by points P1 and P2 on the bifurcation diagram. P1 lying above the Turing curve is diffusionally stable and P2 inside the Turing region is unstable.

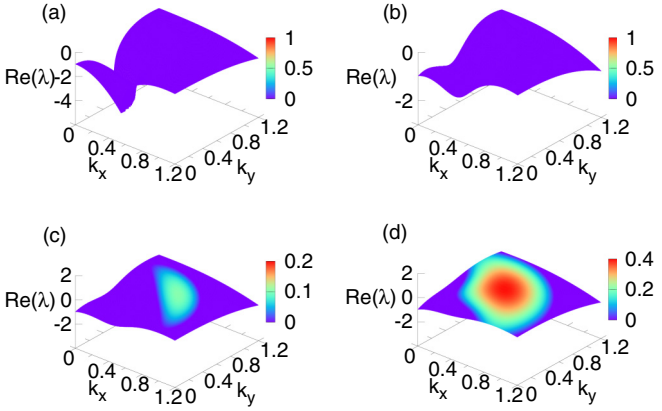

FIG. 5. Three-dimensional dispersion diagram for thermodiffusion induced instability in the presence of diffusive transport: plot of real part of the growth rate Re(λ) as a function of k_x and k_y obtained from linear stability analysis for different values of the imposed temperature gradient : (a) $\nabla T = 0$, (b) $\nabla T = 3.0$, (c) $\nabla T = 4.0$, and (d) $\nabla T = 6.0$. The parameters' values are corresponding to point P1 with Soret coefficients taken as $S_{T_u} = S_{T_v} = 0.1$.

Turing condition: $(3da^2 - 5ab - 125d)^2 = 100abd(a^2 + 25)$ as derived from the linear stability analysis. In Fig. 4, we plot the Hopf (blue with solid circles) and Turing (red with solid squares) bifurcation curves for $\sigma = 10.0$ and $d = 1.6$, to depict the regions of instabilities that separate out the region of homogeneous stable steady state (the region above the Hopf bifurcation line) from oscillatory unstable state and the region of inhomogeneous Turing pattern (the region above the Hopf bifurcation curve and below the Turing bifurcation curve). When $\sigma = 1.0$, the Hopf-bifurcation curve lies well above the Turing curve and thus if we choose a stable steady state at relatively high b value, i.e., large $[ClO_2]/[I_2]$, it does not come under the Turing region of instability and thereby no stationary patterns could be observed. Therefore, increasing σ, the Hopf curve shifts downward proportionally and a stable steady state with lower values of b can become unstable to show diffusion-driven instability. Here, the homogeneous stable steady state depicted by point P1(18.0,1.7) in the bifurcation diagram shown in Fig. 4 lies above the Turing curve and is stable in the presence of diffusion and the steady state denoted by point P2(18.0,1.4) lies inside the Turing region and shows diffusion-driven instability.

We evaluate the growth rate of perturbation, i.e., the real part of the eigenvalue

$$\mathrm{Re}(\lambda_\pm) = [\{f_u + \sigma g_v - (\sigma d + 1)k^2\} \pm R]/2, \qquad (18)$$

that determines the nature of the stability of the steady states. Here, $R = \sqrt{(A + \sqrt{A^2 + B^2})/2}$ with $A = [f_u + \sigma g_v - (\sigma d+1)k^2]^2 - 4\sigma[(f_u g_v - g_u f_v) - (df_u + g_v)k^2 + dk^4] - (\nabla T)^2 (S_{T_u} M_u - \sigma d S_{T_v} M_v)^2 p^2$ and $B = 2p\nabla T[f_u + \sigma g_v - (\sigma d + 1)k^2][S_{T_u} M_u + \sigma d S_{T_v} M_v] - 4p\sigma \nabla T[g_v S_{T_u} M_u + d f_u S_{T_v} M_v - dk^2(S_{T_u} M_u + S_{T_v} M_v)]$.

In Fig. 5, we analyze the stability of a homogeneous stable steady state (P1) by plotting a three-dimensional (λ, k_x, k_y) dispersion diagram in the presence of a thermal gradient ∇T. Since we do not have a prior knowledge of the sign of Soret coefficients of the component ions of the present system, we first proceed by considering the same sign and magnitude of S_{T_u} and S_{T_v} to draw the dispersion curves as illustrated in Fig. 5. Later, we will examine the effect of opposite signs and difference in magnitude of the Soret coefficients in determining the spatiotemporal instabilities if any. The values of other parameters, $d = 1.6$, $\sigma = 10.0$, $\chi_0 = 1.0$, and $k_s = 1.0$, remain fixed throughout our present study unless otherwise mentioned. In the absence of thermal gradient ($\nabla T = 0$), or for smaller values $\nabla T = 3.0$, the real part of the growth rate Re(λ) remains negative as shown by the dispersion diagrams in Figs. 5(a) and 5(b). With higher values of applied thermal gradients we see a shift of the dispersion curve [Fig. 5(c)] and existence of positive eigenvalues Re(λ) for a reasonable combination of k_x and k_y, which indicates the instability generated due to the influence of thermodiffusion. With further increase of the applied thermal gradient, growth rate of perturbation begins to increase as shown by the larger region of positive eigenvalues in the 3D-dispersion diagrams [Fig. 5(d)]. This observation suggests that thermodiffusion-induced spatiotemporal patterns may exist for this parametric space.

We now perform detailed numerical integration of Eq. (16) and Eq. (17) in two dimensions for several values of imposed thermal gradient. For numerical simulations, explicit Euler method is used following a discretization of space and time. A finite system size of length $L_x = L_y = 100$ with grid size $\Delta x = \Delta y = 0.5$ and a time interval $dt = 0.001$ are set for the present purpose. We maintain a no-flux boundary condition throughout our present study. The system is initialized at each mesh point (200×200 array) by perturbing the steady state with $\pm 1\%$ random noise in order to break the initial spatial symmetry. The numerical simulations are performed for long time to ascertain the formation of stable heterogeneous patterns.

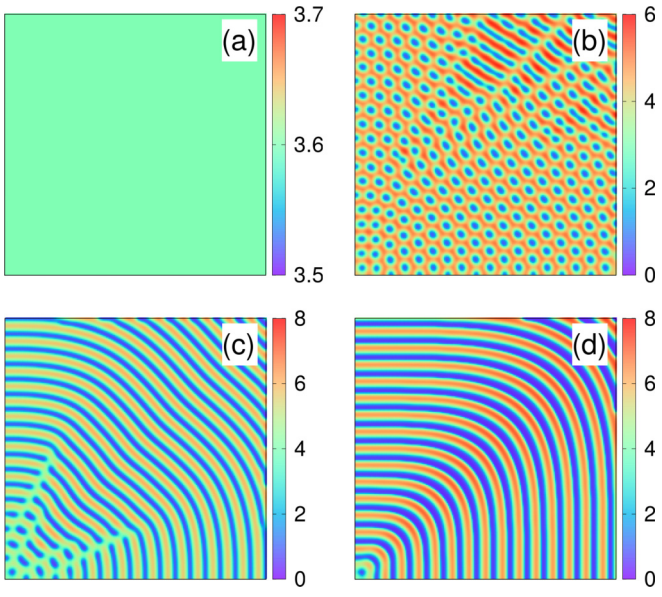

FIG. 6. Thermodiffusion induced stationary patterns for different values of imposed constant temperature gradients. Numerically simulated spatial patterns for the parameter values corresponding to point P1 for (a) $\nabla T = 0$, (b) $\nabla T = 4.0$, (c) $\nabla T = 6.0$, and (d) $\nabla T = 10.0$. A modification of stationary pattern occurs from spot to stripe with increasing values of ∇T. All other parameter values are kept fixed as mentioned in the main text. Red refers to the higher values of concentration of iodide I^-.

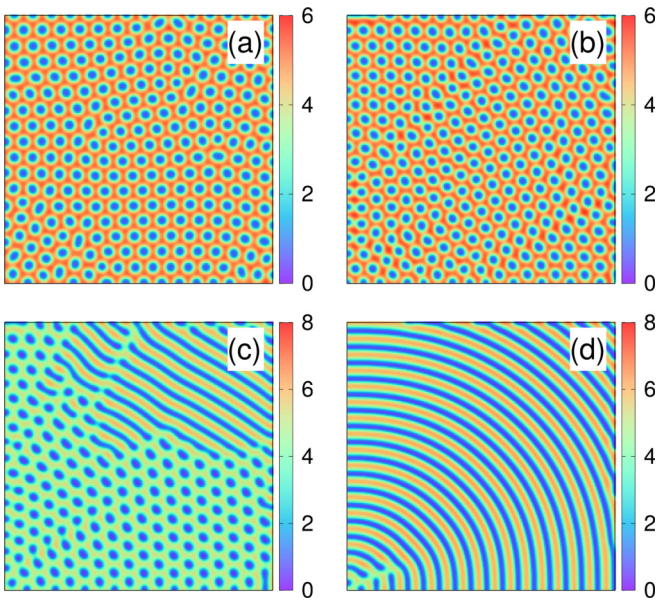

FIG. 7. Thermodiffusion induced transition of stationary patterns from stable spots to stripelike heterogeneous patterns for the parameter values $a = 18.0$, $b = 1.4$ with the increase in the applied temperature gradient: (a) $\nabla T = 0.0$, (b) $\nabla T = 2.0$, (c) $\nabla T = 3.0$, and (d) $\nabla T = 5.0$. All the other parameters are kept the same as described in the main text. Red refers to the higher values of concentration of iodide I^-.

1. Emergence of stationary patterns: Soret coefficients of same sign

We begin our study by considering that both the activator and inhibitor ions are moving in the same direction with equal speed towards the cooler end under the presence of constant temperature gradient, i.e., Soret coefficients are both positive and equal ($S_{T_u} = S_{T_v} = 0.1$). Our numerical simulation results demonstrate that the homogeneous stable steady state corresponding to P1($a = 18.0, b = 1.7$) remains spatially uniform in the absence of imposed thermal gradient as depicted in Fig. 6(a). With the application of a constant thermal gradient ∇T the homogeneous stable steady state becomes unstable resulting in Turing-type stationary spatial instability as illustrated in Fig. 6. We observe, as the value of ∇T systematically increases, a transition of stationary pattern occurs from stable spots [Fig. 6(b)] to stable heterogenous stripelike heterogeneity [Figs. 6(c) and 6(d)]. It is apparent from our numerical simulation results that fluxes originating from thermodiffusion widen up the Turing region of instability leading to the formation of stationary patterns.

To further explore the effect of constant ∇T on modulating stationary Turing patterns, we numerically simulate the reaction-diffusion system described by Eq. (16) and Eq. (17) for a different set of parameters ($a = 18.0, b = 1.4$) as designated by the point P2 that lies inside the Turing region in the bifurcation diagram (Fig. 4). In the absence of any imposed temperature difference, the reaction-diffusion system shows basic Turing instability which results in a stable spotlike stationary pattern for the aforementioned values of the parameters as depicted in Fig. 7(a). With systematic increase of the applied constant ∇T, we observe a modification or deformation occurs in the nature of spot pattern as demonstrated in Fig. 7. A finer look through the time evolution of the instabilities suggests an unstable spot-stripe mixture obtained for an intermediate value of $\nabla T = 3.0$, which stems from a competition between different modes of spatial periodicity. We here show a long-time snap of the mixed patterned state in Fig. 7(c). Further increase in ∇T ultimately results in a stable stripeslike heterogeneity as depicted in Fig. 7(d).

In order to investigate what happens if the movement of both the ions is towards the hot end of the reaction chamber, i.e., Soret coefficients are negative but equal in magnitude ($S_{T_u} = S_{T_v} = -0.1$), we carry out numerical simulations as before with the same parameter set. In what follows, we observe that in the case of both the activator and inhibitor ions having the same sign of Soret coefficients (either positive or negative), thermodiffusion can lead to the formation of stationary spatial patterns and modulation of Turing instability from a spotlike patterned state to finally stripelike heterogenous stationary patterns. Further analysis of the dispersion diagram reveals that no oscillatory instability is possible in this case since the real part of the growth rates always dominates over the imaginary ones (we do not present the results here for the sake of brevity).

It is apparent that if the Soret coefficient of species is high, a lesser value of thermal gradient will be required to initiate pattern formation for a fixed value of phenomenological constant k_s. To get a quantitive estimate of ∇T required for stationary pattern formation, we proceed as follows. The condition on the dispersion relation for a transition to a stationary pattern is $\lambda = 0$ with $\mathrm{Im}(k = 0)$, so the perturbation has the

form $e^{i\mathbf{k}\cdot\mathbf{r}}$ with a purely imaginary exponent. Setting $\lambda = 0$ in Eq. (12) yields $h = 0$. In order to get an analytical estimate for the same, we assume $k_x = k_y = q$, i.e., both the directions equally contribute to the growth rate of the perturbation. While doing so we get the following equation:

$$\sigma(f_u g_v - g_u f_v) - \sigma(df_u + g_v)k^2 + \sigma\, dk^4 + ip\sigma\nabla T[(S_{T_u}M_u g_v + dS_{T_v}M_v f_u) - dk^2(S_{T_u}M_u + S_{T_v}M_v)] - \sigma d p^2 S_{T_u}S_{T_v}M_u M_v(\nabla T)^2 = 0. \quad (19)$$

Setting the imaginary part equal to zero yields the condition $q_c^2 = [g_v S_{T_u}M_u + df_u S_{T_v}M_v]/[2d(S_{T_u}M_u + S_{T_v}M_v)]$ for the bifurcation to stationary pattern. We substitute the values of q_c in Eq. (19), which on rearrangement leads to the following expression for the thermal gradient:

$$\nabla T^2 = \frac{d\left(q_c^2\right)^2 - 2(df_u + g_v)q_c^2 + (f_u g_v - g_u f_v)}{4dS_{T_u}S_{T_v}M_u M_v q_c^2}. \quad (20)$$

For $k_x = k_y = q$, we expect stationary patterns to exist for a thermal gradient equal to or greater than this value. From this relation it is evident that, if the product of the Soret coefficients is high, lower values of thermal gradient can create stationary patterns. To verify the above prediction obtained for the value of ∇T for the isotropic case ($k_x = k_y = q$), we ran a few numerical simulations by varying the values of S_T [lower (0.05) and higher (0.2)] and find out that it is consistent with the prediction that a higher value of ∇T is required to initiate a stationary pattern and vice versa (results are not shown for the sake of brevity). To get a better insight of how ∇T varies with S_T and k_s, we draw a three-dimensional diagram (S_T, k_s, ∇T) as shown in Fig. S1 in the Supplemental Material [50].

2. *Emergence of propagating spots and stripes: Soret coefficients of opposite sign*

To get a better insight of how and to what extent the direction of the movement of the ions under thermodiffusion might affect the spatiotemporal dynamics, we next proceed by considering opposite signs of Soret coefficients such that $S_{T_u} = 0.1$ and $S_{T_v} = -0.1$. This suggests that activator and inhibitor ions are moving in opposite directions in the presence of a constant temperature gradient. We repeat the numerical simulations for the aforementioned parameter sets designated by point P1 ($a = 18.0, b = 1.7$), keeping all the other parameters the same as before. At this parameter set, the system remains spatially homogeneous in the absence of any temperature gradient, i.e., $\nabla T = 0$, as shown in Fig. 8(a). As we systematically increase the applied constant thermal gradient, we observe emergence of spatiotemporal instability in the form of moving mixed spots and stripes for lower values of $\nabla T = 3.3$, as shown in Fig. 8(b) and demonstrated in Movie 2 (see Supplemental Material [50]). Further increase in ∇T leads to a transition to a traveling striped pattern [Fig. 8(c)]. The corresponding video is illustrated in Movie 3 in the Supplemental Material [50]. A closer look into the time evolution of traveling patterns reveals that there is a competition between the direction of movement of the traveling waves for a higher value of $\nabla T \geqslant 4$. We observe changes in the direction of the moving patterns which need a detailed nonlinear analysis which is beyond the scope of our present study.

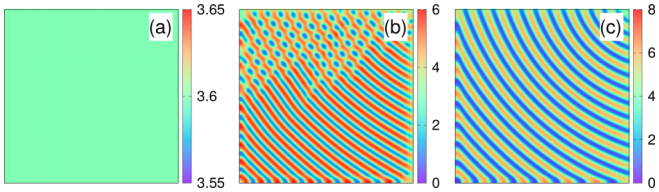

FIG. 8. Thermodiffusion induced spatiotemporal instability: moving patterns for the parameter values $a = 18.0$, $b = 1.7$, $S_{T_u} = 0.1$, $S_{T_v} = -0.1$ for applied temperature gradient of values: (a) $\nabla T = 2.0$, (b) $\nabla T = 3.3$, and (c) $\nabla T = 5.0$. Red refers to the higher values of concentration of iodide I^-. All the other parameters are kept the same as described in the main text.

To further check the impact of the imposed thermal gradient on the region of Turing instability when the activator and inhibitor have the same magnitude but opposite signs of Soret coefficients ($S_{T_u} = 0.1, S_{T_v} = -0.1$), we numerically simulate the spatiotemporal dynamics for the parameter values $a = 18.0, b = 1.4$ corresponding to the point P2 (lies inside the Turing region) in the bifurcation diagram in Fig. 4. Similar to our previous observation, wave instability arises in the form of moving spots or stripes from a stationary Turing instability as demonstrated by longtime snaps in Fig. 9. For smaller values of imposed constant thermal gradients, $\nabla T = 1.0$, the morphology of the pattern still remained intact but the nature of the pattern changes from stationary spots to propagating spots [Fig. 9(a) and Movie 4 (see Supplemental Material at [50])]. Further increase of $\nabla T = 3.0$ leads to the transition from moving spots to traveling stripes [Fig. 9(b) and Movie 5 in [50]]. We observe that spots start to aggregate and develop traveling stripes with the increase of ∇T.

To this end, it is important to mention that one can vary the initial total concentration of the reactants χ_0 and get a different set of parameter region for thermodiffusion-driven instabilities. However, our results remain consistent with the basic observations we have obtained so far. The values of Soret coefficients for ionic species are nearly equal but the signs might be different. In general, Soret coefficients are of

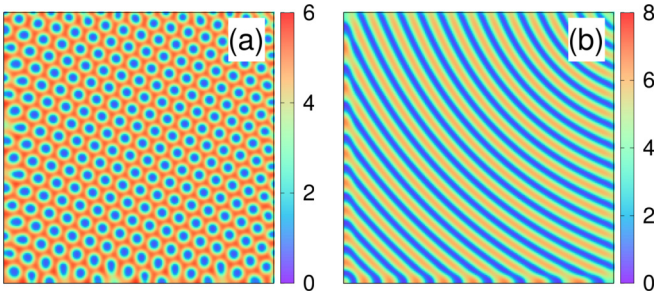

FIG. 9. Thermodiffusion induced spatiotemporal instability: moving patterns for the parameter values $a = 18.0$, $b = 1.4$, $S_{T_u} = 0.1$, $S_{T_v} = -0.1$ with the increase of the applied temperature gradients of values: (a) $\nabla T = 1.0$ (moving spots); (b) $\nabla T = 3$ (moving stripes). Red refers to the higher values of concentration of iodide I^-. All the other parameters are kept the same as described in the main text.

order $\simeq 10^{-3} - 10^{-1}$ K^{-1} [31], whereas larger values of Soret coefficients are found in polymeric solutions $S_T \simeq 0.5$ K^{-1}. Recently, in colloidal solutions, values of S_T from 0.17 to 0.25 K^{-1} have been reported [52]. In the present work, since we do not have any prior experimental studies on S_T of iodide and chlorite ions in the CDIMA reaction-diffusion system, we consider each of the possible combinations (all the results are not shown here for the sake of brevity). In this regard, we furthermore check if Soret coefficients are of different magnitude; for example, the activator is slow compared to the inhibitor subjected to the constant thermal gradient in the system, i.e., $S_{T_u} = 0.05$ and $S_{T_v} = 0.1$. In this case, instead of having stationary patterns as previously seen for the same sign of Soret coefficients and for the parameters described by point P1, we always get either transient waves or propagating spots or stripes as demonstrated in Movies 6 and 7 (see Supplemental Material [50]). In what follows, we can conclude that the case of the same signs of Soret coefficients results in stationary patterns. On the other hand, opposite signs or difference in the magnitude of Soret coefficients generates spatiotemporal instabilities in the form of transient waves, stable moving spots, or traveling stripes.

3. Thermodiffusion alone is inadequate to produce Turing instability in a CDIMA system

At this juncture, we investigate whether the applied constant thermal gradient is sufficient to create Turing instability in the CDIMA system in the absence of diffusion driven instability. The dispersion diagram, i e., plot of the real and imaginary part of the eigenvalues with respect to k_x and k_y, suggests that, under the condition $d = 1, \sigma = 1.0$, there is very little possibility of stationary spatial pattern formation as the region of homogeneous stable steady state is separated by a wide oscillatory region before it hits the Turing curve, as illustrated in the bifurcation diagram [Fig. 10(a)]. One important observation from our numerical studies is that, with no disparity in the ratio of diffusion coefficients and without the aid of starch in the reaction medium, i.e., $d = 1.0$ and $\sigma = 1.0$, thermodiffusion solely is not enough to create stationary Turing-like patterns. Nevertheless, for the parameter values described by point P1 ($a = 18.0, b = 1.7$) in the bifurcation diagram depicted in Fig. 10(a), we observe formation of stable spiral waves in the absence of applied thermal gradient. The corresponding image is shown in Fig. 10(b). However, in the case of the component having same sign and magnitude of Soret coefficients ($S_{T_u} = S_{T_v} = 0.1$), we observe that spiral waves show a drift motion towards the boundary in the presence of a nonzero thermal gradient ($\nabla T = 1.0$), as illustrated in Figs. 10(c)–10(h) in successive time snaps. Numerical simulation results reveal a conspicuous feature of these spiral waves: these waves while drifting towards the boundaries might diminish a later time as shown in Movie 8 (see [50]). If the ionic components move towards the hot end of the reaction vessel (i.e., both the Soret coefficients are negative), there is also formation of similar spiral waves which finally disappear at longer times.

On the other hand, for opposite signs of Soret coefficients ($S_{T_u} = 0.1, S_{T_v} = -0.1$) or ($S_{T_u} = -0.1, S_{T_v} = 0.1$), i.e., two ionic species moving in opposite directions under a constant

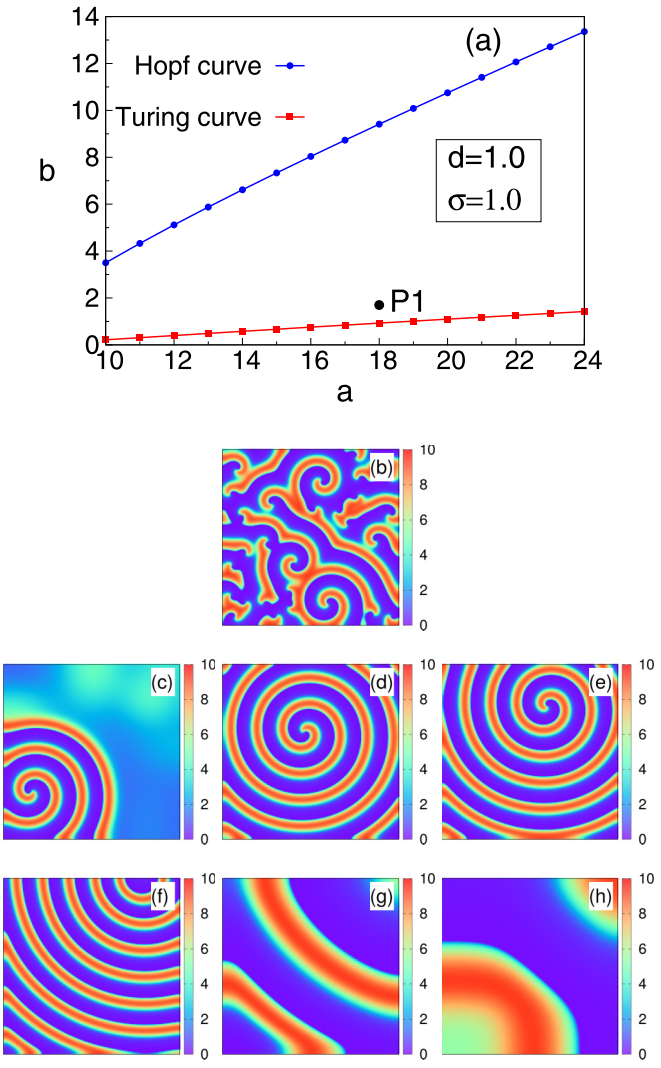

FIG. 10. Spatiotemporal instability for equal diffusivity: (a) plot of $b - a$ bifurcation diagram when diffusion coefficients of activator and inhibitor ions are equal and starch is absent in the medium, i.e., $d = 1$, $\sigma = 1$. (b) Snapshot of numerically simulated concentration profile of iodide (I^-) in the absence of thermal gradient for the parameter values $a = 18.0$, $b = 1.7$, $S_{T_u} = 0.1$, $S_{T_v} = 0.1$ and simulated in a domain of size (200×200) with spatial grid $\Delta x = \Delta y = 0.5$. Successive snapshots of concentration profiles in the presence of applied temperature gradients ($\nabla T = 1.0$) are shown in successive figures from (c) to (h). In this case, we consider a domain size (200×200) with a larger spatial grid $\Delta x = \Delta y = 1.0$. All the other parameters are kept the same as described in the main text. Red signifies high concentration of iodide ions.

thermal gradient, we observe formation of spirals as shown by the longtime snapshots in Fig. 11. Interestingly, in this case, the spiral pattern is stable and does not show drift motion.

To this end, we discuss the effect of domain size and grid spacing which might have an impact on wave instabilities. However, by increasing the domain size to 200×200 or decreasing the grid spacing to $\Delta x = \Delta y = 0.4$, we do not find any modulation of the wavelength or frequency in the case of stationary patterns and propagating Turing type spots or stripes. The nature and morphology of the patterns also

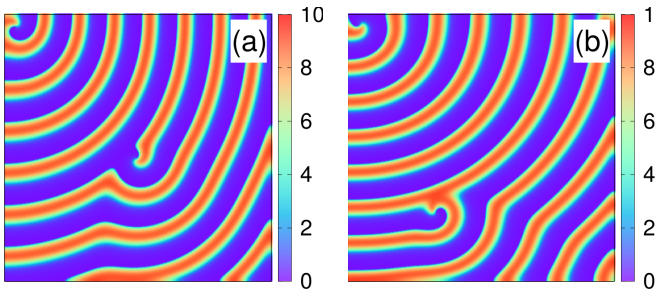

FIG. 11. Thermodiffusion induced spiral waves for opposite signs of Soret coefficients: shown is the snapshot of spiral patterns for the parameter values $a = 18.0$, $b = 1.7$, $\nabla T = 1.0$ and the Soret coefficients are (a) $S_{T_u} = 0.1$, $S_{T_v} = -0.1$; (b) $S_{T_u} = -0.1$, $S_{T_v} = 0.1$. The domain size is (200×200) with spatial grid $\Delta x = \Delta y = 0.5$. Red refers to high concentration of iodide ions I^-. All the other parameters are kept the same as described in the main text.

remained similar as we find for the smaller domain size or with larger grid spacing. However, there is a conspicuous effect of boundary and spatial grids in the case of spiral wave formation. We find that a larger domain (200×200 or 400×400) in general helps to hold spiral waves. But at the same time the effect of the spatial grid is peculiar. We find that a smaller spatial grid is effective in the generation of spiral waves but it might lead to broken spiral waves. A relatively larger grid size helps to sustain unbroken spiral arms in general. For example, if we numerically simulate using a large grid size 1.0, and large domain size (400×400) corresponding to Fig. 11(a), we initially observe formation of a small spiral center surrounded by target waves which later on converts to a stable spiral wave pattern as demonstrated in Movie 9 (see Supplemental Material [50]).

IV. CONCLUDING REMARKS

The presence of temperature gradients in a natural environment is common and its use in chemical systems has come up quite effectively in the recent past [35,36,38–40,43,44]. In this paper, we show that thermodiffusion, i.e., mass flow driven by thermal gradients, can be utilized in creation and modification of spatiotemporal instabilities. As a prototypical model we consider the Brusselator model and CDIMA system, which have been extensively studied for pattern formation. Under the influence of thermodiffusion, these two models show formation of a large variety of spatiotemporal instabilities. In the case of the Brusselator model, even with equal diffusivities of the components ionic species but having unequal Soret coefficients, i.e., differential movement of the components towards cooler region under thermal gradient, one can achieve formation of stationary Turing-like patterns. Using an external thermal gradient one can overcome the stringent requirement of disparity of diffusion coefficients for Turing pattern formation. However, for the same case, if any of the components has negative Soret coefficient spatiotemporal dynamics shows evolution of propagating waves. On the other hand, formation of such stationary patterns requires the same sign and magnitude of Soret coefficients of the constituent activator and inhibitor ionic species in a CDIMA system in the presence of starch in the medium. This is attributed to the movement of the ions in the same direction with equal speed under thermodiffusion. This supports the fact of nearly equal Soret coefficients for ionic species. Interestingly, either the difference in sign or in magnitude lead to the development of wave instabilities such as propagating spatial patterns of spot or stripes. Moreover, larger values of thermal gradients lead to the formation of stripelike heterogeneity. This stems from the fact of differential thermodiffusion of the two components, which causes the symmetry breaking resulting wave instabilities. We also find that thermodiffusion solely is inadequate to generate Turing instabilities in the case of a CDIMA system with equal diffusivities and without starch in the medium. However, we see formation of spiral waves having drift motion and their disappearance in long times under a no-flux boundary condition.

Keeping in view of recent developments, experimental observation of thermodiffusion-induced unpinning of three-dimensional scroll waves has been reported in the Belousov-Zhabotinsky reaction-diffusion system [44]. Although the present study of pattern formation and modulation by thermal gradient has been carried out on specific models as prototypical examples, we believe that our results on thermodiffusion-induced spatiotemporal instabilities are likely to be important for other reaction-diffusion systems of activator-inhibitor type. In summary, application of an external thermal gradient provides us an opportunity to achieve a large variety of spatiotemporal instabilities. Our study can be extended to see how thermal gradients influence the spatiotemporal dynamics of microorganisms or synthetic active systems and opens up new possibilities to carry out experiments of pattern formation beyond Turing space.

ACKNOWLEDGMENT

P.G. would like to acknowledge the financial support from Department of Science and Technology India, INSPIRE Faculty Award (Grant No. IFA15/CH-201).

[1] J. D. Murray, *Mathematical Biology: II: Spatial Models and Biomedical Applications*, 3rd ed. (Springer, New York, 2003), Vol. 18.

[2] M. C. Cross and P. C. Hohenberg, Rev. Mod. Phys. **65**, 851 (1993).

[3] I. R. Epstein and J. A. Pojman, *An Introduction to Nonlinear Chemical Dynamics: Oscillations, Waves, Patterns, and Chaos* (Oxford University Press, New York, 1998).

[4] M. Cross and H. Greenside, *Pattern Formation and Dynamics in Nonequilibrium Systems* (Cambridge University Press, Cambridge, UK, 2009).

[5] A. M. Turing, Philos. Trans. R. Soc., B **237**, 37 (1952).

[6] V. Castets, E. Dulos, J. Boissonade, and P. De Kepper, Phys. Rev. Lett. **64**, 2953 (1990).

[7] I. Lengyel and I. R. Epstein, Science **251**, 650 (1991).

[8] P. K. Maini, K. J. Painter, and H. N. P. Chau, J. Chem. Soc., Faraday Trans. **93**, 3601 (1997).
[9] Q. Ouyang and H. L. Swinney, Nature (London) **352**, 610 (1991).
[10] B. Rudovics, E. Barillot, P. W. Davies, E. Dulos, J. Boissonade, and P. De Kepper, J. Phys. Chem. A **103**, 1790 (1999).
[11] S. Kondo and T. Miura, Science **329**, 1616 (2010).
[12] A. B. Rovinsky and M. Menzinger, Phys. Rev. Lett. **70**, 778 (1993).
[13] B. Schmidt, P. De Kepper, and S. C. Müller, Phys. Rev. Lett. **90**, 118302 (2003).
[14] S. S. Riaz, S. Kar, and D. S. Ray, J. Chem. Phys. **121**, 5395 (2004).
[15] S. S. Riaz, S. Banarjee, S. Kar, and D. S. Ray, Eur. Phys. J. B **53**, 509 (2006).
[16] S. Dutta and D. S. Ray, Phys. Rev. E **75**, 016205 (2007).
[17] A. Giri and S. Kar, J. Chem. Phys. **150**, 094904 (2019).
[18] M. Dolnik, A. M. Zhabotinsky, and I. R. Epstein, Phys. Rev. E **63**, 026101 (2001).
[19] P. Ghosh, S. Sen, S. S. Riaz, and D. S. Ray, Phys. Rev. E **79**, 056216 (2009).
[20] S. Sen, P. Ghosh, S. S. Riaz, and D. S. Ray, Phys. Rev. E **80**, 046212 (2009).
[21] P. Ghosh, Phys. Rev. E **84**, 016222 (2011).
[22] F. Sagués, J. M. Sancho, and J. García-Ojalvo, Rev. Mod. Phys. **79**, 829 (2007).
[23] S. S. Riaz, S. Dutta, S. Kar, and D. S. Ray, Eur. Phys. J. B **47**, 255 (2005).
[24] D. Das and D. S. Ray, Phys. Rev. E **87**, 062924 (2013).
[25] D. Karig, K. M. Martini, T. Lu, N. A. DeLateur, N. Goldenfeld, and R. Weiss, Proc. Natl. Acad. Sci. USA **115**, 6572 (2018).
[26] T. Biancalani, D. Fanelli, and F. Di Patti, Phys. Rev. E **81**, 046215 (2010).
[27] T. Butler and N. Goldenfeld, Phys. Rev. E **80**, 030902(R) (2009).
[28] D. Fanelli, C. Cianci, and F. Di Patti, Eur. Phys. J. B **86**, 142 (2013).
[29] M. Asllani, J. D. Challenger, F. S. Pavone, L. Sacconi, and D. Fanelli, Nat. Commun. **5**, 4517 (2014).
[30] J. K. Platten and P. Costesèque, Eur. Phys. J. E **15**, 235 (2004).
[31] J. K. Platten, J. Appl. Mech. **73**, 5 (2006).
[32] S. Duhr and D. Braun, Proc. Natl. Acad. Sci., USA **103**, 19678 (2006).
[33] J. A. Bierlein, J. Chem. Phys. **23**, 10 (1955).
[34] S. Srinivasan and M. Z. Saghir, Int. J. Therm. Sci. **50**, 1125 (2011).
[35] P. C. Mangelsdorf, J. Chem. Phys. **32**, 293 (1960).
[36] S. Wiegand, J. Phys.: Condens. Matter **16**, R357 (2004).
[37] F. Huang, P. Chakraborty, C. C. Lundstrom, C. Holmden, J. J. G. Glessner, S. W. Kieffer, and C. E. Lesher, Nature (London) **464**, 396 (2010).
[38] H. Ning, J. K. G. Dhont, and S. Wiegand, Langmuir **24**, 2426 (2008).
[39] D. Vigolo, R. Rusconi, H. A. Stone, and R. Piazza, Soft Matter **6**, 3489 (2010).
[40] J. Lenglet, A. Bourdon, J. C. Bacri, and G. Demouchy, Phys. Rev. E **65**, 031408 (2002).
[41] W. Köhler, J. Chem. Phys. **98**, 660 (1993).
[42] B.-J. de Gans, R. Kita, B. Müller, and S. Wiegand, J. Chem. Phys. **118**, 8073 (2003).
[43] S. Dutta and D. S. Ray, Phys. Rev. E **75**, 066206 (2007).
[44] N. P. Das, D. Mahanta, and S. Dutta, Phys. Rev. E **90**, 022916 (2014).
[45] I. Lengyel, S. Kádár, and I. R. Epstein, Phys. Rev. Lett. **69**, 2729 (1992).
[46] I. Lengyel and I. R. Epstein, Acc. Chem. Res. **26**, 235 (1993).
[47] R. Piazza and A. Guarino, Phys. Rev. Lett. **88**, 208302 (2002).
[48] I. Prigogine and R. Lefever, J. Chem. Phys. **48**, 1695 (1968).
[49] J. J. Tyson, J. Chem. Phys. **58**, 3919 (1973).
[50] See Supplemental Material at http://link.aps.org/supplemental/10.1103/PhysRevE.100.042217 for the video and figure files described in the main text.
[51] P. Ghosh and D. S. Ray, J. Chem. Phys. **135**, 104112 (2011).
[52] E. Bringuier and A. Bourdon, Phys. Rev. E **67**, 011404 (2003).